Modeling of wave shoaling in a 2D-NWT using a spilling breaker model *

Stéphan Guignard and Stéphan T. Grilli
Department of Ocean Engineering, University of Rhode Island, Narragansett, RI 02882, USA

ABSTRACT

A 2D fully nonlinear NWT modeling wave propagation over arbitrary bottom topography is extended by the addition of a spilling breaker model, in which an absorbing surface pressure is specified over breaking wave crest areas. The instantaneous power dissipated for each breaking wave by the absorbing pressure is specified proportional to the dissipation in an inverted hydraulic jump of identical characteristics. These are obtained by applying a wave tracking algorithm to each calculated free surface. A maximum surface slope breaking criteria is used to identify breaking waves within the incident wave train. Computations for a periodic wave shoaling and breaking over a plane slope are compared to laboratory experiments. The agreement is quite good, although more work remains to be done in refining the breaker model parameter.

Keywords : Nonlinear nearshore wave transformations, wave shoaling and breaking, numerical wave tank, breaker model, boundary element method.

INTRODUCTION

Over the past two decades, increasingly accurate models (i.e., Numerical Wave Tanks; NWT) have been developed for calculating nearshore wave propagation. Most of these models were based on inviscid, irrotational (i.e., potential), flow theory, and their predictions were shown to be in good agreement with well-controlled laboratory experiments, for wave shoaling over mild slopes, up to the initial stages of crest overturning (e.g., Grilli *et al.*, 1994, 1997). Three main approaches were followed in these models : (i) the direct solution of Fully Nonlinear Potential Flow (FNPF) equations, typically, in an Eulerian-Lagrangian formulation, either in a periodic or a conformally mapped space (e.g., Longuett-Higgins and Cokelet, 1976; Vinje and Brevig, 1981, Dold and Peregrine, 1986), or in the physical space (e.g., Grilli *et al.*, 1989); (ii) the derivation and solution of approximate depth-integrated long wave equations, based on FNPF theory, such as Boussinesq equations with improved dispersion and nonlinear characteristics (e.g., Wei *et al.*, 1995); and (iii) the direct solution of Euler/Navier-Stokes equations, using a domain discretization method, such as Volume of Fluids (VOF; Lin and Liu, 1998; Guignard *et al.*, 2001) or Marker and Cell (MAC; Raad, 1995), with and without turbulence models.

Approach (i) does not make any approximation of FNPF equations (other than a discretization) and can model the overturning of one wave, up to impact of the breaker jet on the free surface (e.g., Grilli and Subramanya, 1996; Grilli *et al.*, 1997). It is however quite computationally expensive (as compared to approach (ii)), and does not naturally include energy dissipation terms (representing bottom friction or wave breaking effects). Approach (ii) only approximately solves FNPF equations, and depth integration precludes modeling steep bottom obstacles. But it is less computationally demanding and can accommodate energy dissipation terms globally representing wave breaking (Karambas and Koutitas, 1992; Schäffer *et al.*, 1993; Nadaoka and Ono, 1999; Skotner and Apelt, 1999ab; Veeramony and Svendsen, 1999, 2000; Kennedy *et al.*, 2000). Approach (iii) is very computationally expensive and suffers from significant numerical diffusion, which both prevent accurately modeling wave shoaling over long propagation distances. However, when coupled with accurate free surface tracking algorithms, it can provide details of the flow together with the complex shape of post-breaking waves (e.g., Guignard *et al.*, 2001). Note the recent, more efficient, coupling of approaches (i) and (iii) proposed by Guignard *et al.* (1999).

In many coastal engineering problems, it is necessary to compute nonlinear characteristics of waves shoaling over mildly sloping bottom, up to the breaking point. While, in such cases, it is important to account for the energy dissipation (and thus the reduction in wave reflection) resulting from wave breaking in the surf zone, a global approach can be used in which the details of the flow within breaking waves

*To appear in *Proc. ISOPE 2001 Conf.* (Stavanger, Norway)

are not sought nor modeled. Models related to approach (iii) above could provide such details, but both the computational cost would be too high and the shoaling part of wave propagation would be less accurately computed, due to numerical diffusion, than when using a NWT based on FNPF theory (e.g., Guignard *et al.*, 1999, 2001). To apply FNPF-NWTs to such problems, many researchers implemented so-called "absorbing beaches" at the far end of their NWTs, in which, usually, a surface pressure distribution working against incident waves is specified. This both prevents wave overturning from occurring and absorbs incident wave energy (see reviews and results in, e.g., Clément, 1996, and Grilli and Horrillo, 1997a). Absorbing beaches work well for periodic or nearly periodic waves, propagating over constant depth or mildly sloping bottom. For irregular incident waves, wave groups, and/or irregular bathymetry (such as barred-beaches), it is desirable to also have a simple and efficient means of preventing wave overturning (which may occur anywhere and typically terminates FNPF computations), while absorbing the energy of individual breaking waves, in relation with the physical rate of energy dissipation occurring in actual waves. Wang *et al.* (1995), for instance, suppressed breaking in their so-called "longtank" computations, by peeling water away from wave crests reaching a limiting height. This *ad-hoc* numerical method, however, violates continuity equation and has no physical justification.

For spilling breakers over mild slopes, breaking is usually limited to overturning in the high crest area and leads to the formation of a "roller", while the bulk of the wave flow keeps potential-like features (e.g., Cointe and Tulin, 1994). When the roller forms, the wave front face steepens and then reaches a rather constant slope during breaking, while wave height continuously decreases due to energy dissipation. These properties of spilling breakers are the basis for the "maximum front slope" breaking criteria used by Schäffer *et al.* (1993), and many others, in long wave models, in combination with empirical eddy viscosity terms in the momentum equation, calibrated based on laboratory experiments. In the present work, we use the two-dimensional (2D) FNPF-NWT initially developed by Grilli *et al.* (1989) (GSS), with its later improvements described in the next section, to study nearshore wave propagation (Fig. 1). Long wave models cannot predict breaking and thus need additional empirical information. By contrast, FNPF-NWTs can model overturning waves and thus accurately predict breaking locations and types : spilling, plunging, or surging (Grilli *et al.*, 1997). Computations, however, are terminated when overturning of one wave occurs. Hence, for spilling breakers, when details of the small size roller are not needed, as done in long wave models, one can globally represent the energy dissipation due to breaking, while not resolving the details of the crest in the model and still assuming potential flow within the waves. Since wave overturning must be prevented, a maximum/minimum front slope empirical criterion, similar to Schäffer *et al.*'s, can be used to determine whether a wave starts or stops breaking and when and where

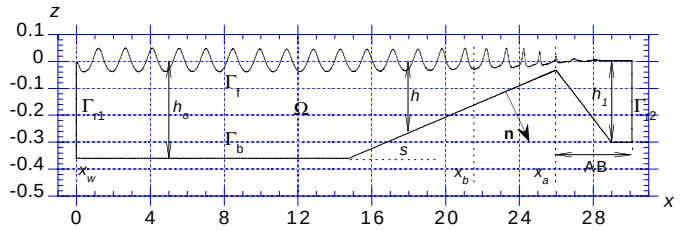

Fig. 1 : Sketch of numerical wave tank for periodic wave shoaling and breaking computations. Note, AB: absorbing beach for $x \geq x_a$; piston wavemaker at $x = x_w$; breaking point at $x = x_b$.

the dissipation should be applied. As in absorbing beaches, a pressure distributed over the crest of breaking waves can be used to specify the energy dissipation. Based on results obtained in the surf zone hydrodynamics research community, the instantaneous rate of energy dissipation for each spilling breaker can be assumed to be that of an inverted hydraulic jump (Svendsen *et al.*, 1978; Svendsen and Madsen, 1984; Svendsen *et al.*, 2001). In our model, the pressure distribution is specified from the point where normal velocity changes sign behind the crest to the similar point on the front face of each breaking wave. The work produced by this pressure against the wave is calibrated in real time to be proportional to the energy dissipation in an hydraulic jump of identical characteristics. This requires knowing values of instantaneous wave height H, celerity c, and depth below crest $h_c = h + H$, and trough, h_t (Fig. 2). Hence, a wave tracking algorithm is developed, in which individual waves are identified and followed throughout their shoaling and breaking in the NWT, while the breaking criteria is being checked. The spilling breaker model parameters are calibrated by comparing results to laboratory experiments for mean wave height H and mean-water-level (MWL) variations, during shoaling of periodic waves generated by a piston wavemaker (Hansen and Svendsen, 1979).

Note that, in recent years, other breaking criteria have been proposed to detect breaking in NWTs. Thus, Subramani *et al.* (1998) developed a maximum surface curvature criteria to identify deep water breaking waves ($\kappa H \leq 0.7$, with κ the crest curvature), and Nadaoka and Ono (1999) and Gentaz and Alessandrini (2000) used a criteria based on a threshold vertical pressure gradient at the free surface ($\frac{\partial p}{\partial z} \geq \rho g$). Such criteria were also tested in the present work, but results presented here are limited to the front slope criteria.

THE NUMERICAL WAVE TANK

Svendsen (1990) (GS) and Grilli and Subramanya (1994) further improved GSS's NWT by addressing important problems, such as surface piercing wavemakers, corner double-node continuity and compatibility conditions, and quasi-singular integrations. Grilli and Subramanya (1996) implemented more accurate discretization methods and a node regridding technique in the NWT, and were able to accu-

rately model breaking solitary waves over mild and steep slopes, up to touch-down of the breaker jet on the free surface. Grilli and Horrillo (1997a) (GH) implemented exact periodic wave generation (streamfunction wave solution), and numerical absorption in the NWT, the latter being achieved through a combination of a surface pressure, working against waves, and open active absorbing boundaries, within an absorbing beach (see also Clément, 1996). They were able to calculate numerically-exact fully nonlinear properties of periodic waves shoaling over mild monotonous slopes, such as wave height and celerity variations (Grilli and Horrillo, 1997b), and wave transformations over barred-beaches (Grilli and Horrillo, 1999). Comparisons of results obtained in this NWT with laboratory experiments indicate that FNPF theory is accurate for modeling solitary wave runup on steep slopes (Svendsen and Grilli, 1990) and shoaling over mild slopes, up to and slightly beyond wave overturning (Grilli *et al.*, 1994, 1997, 1998). Grilli and Horrillo's work also indicates that periodic wave shoaling over barred-beaches is also modeled in the NWT, as compared to laboratory experiments.

Governing equations and boundary conditions

Equations for GSS/GS/GH's two-dimensional FNPF numerical wave tank (NWT) are briefly presented in the following. The velocity potential $\phi(\mathbf{x},t)$ is used to describe inviscid irrotational flows in the vertical plane (x,z) and the velocity is defined by, $\mathbf{u}=\nabla\phi=(u,w)$. Continuity equation in the fluid domain $\Omega(t)$ with boundary $\Gamma(t)$ is a Laplace's equation for the potential (Fig. 1),

$$\nabla^2\phi=0 \qquad \text{in } \Omega(t) \qquad (1)$$

On the free surface $\Gamma_f(t)$, ϕ satisfies the kinematic and dynamic boundary conditions,

$$\frac{D\,\mathbf{R}}{D\,t}=(\frac{\partial}{\partial t}+\mathbf{u}\cdot\nabla)\,\mathbf{R}=\mathbf{u}=\nabla\phi \qquad \text{on } \Gamma_f(t) \qquad (2)$$

$$\frac{D\phi}{Dt}=-gz+\frac{1}{2}\nabla\phi\cdot\nabla\phi-\frac{p_f}{\rho} \qquad \text{on } \Gamma_f(t) \qquad (3)$$

respectively, with $\mathbf{R}$, the position vector on the free surface, g the gravitational acceleration, z the vertical coordinate, p_f the pressure on the free surface, and ρ the fluid density. Along the stationary parts of the boundary such as bottom Γ_b and Γ_{r2}, a no-flow condition is prescribed as,

$$\overline{\frac{\partial\phi}{\partial n}}=0 \qquad \text{on } \Gamma_b,\,\Gamma_{r2} \qquad (4)$$

where the overline denotes specified values.

Various methods have been used for wave generation in this NWT. Here, periodic waves are generated on boundary $\Gamma_{r1}(t)$, either using a solid piston wavemaker moving according to a first-order cnoidal wave solution (GS), or by prescribing numerically exact higher-order streamfunction waves, corrected to specify a zero average mass-flux over one wave period (GH). The first method produces incident intermediate depth waves, similar to those generated in laboratory wave tanks (e.g., Hansen and Svendsen, 1979) and thus can be used for comparing numerical results with experiments. The second method produces more accurate finite amplitude waves, which keep permanent form over constant depth, whereas first-order cnoidal waves may be subject to amplitude modulations, due to higher-harmonic generation (e.g., GH). Thus, for a specified wavemaker or wave motion $\mathbf{x}_w(t)$ on $\Gamma_{r1}(t)$ (Fig. 1), we have,

$$\overline{\mathbf{x}}=\mathbf{x}_w \;\;;\;\; \overline{\frac{\partial\phi}{\partial n}}=\mathbf{u}_w\cdot\mathbf{n}=\frac{\mathrm{d}\mathbf{x}_w}{\mathrm{d}\,t}\cdot\mathbf{n} \qquad \text{on } \Gamma_b(t) \qquad (5)$$

where overlines denote specified values, and the time derivative follows the wavemaker or the wave motion. See references for details.

For well-posed problems, we have, $\Gamma\equiv\Gamma_f\cup\Gamma_b\cup\Gamma_{r1}\cup\Gamma_{r2}$.

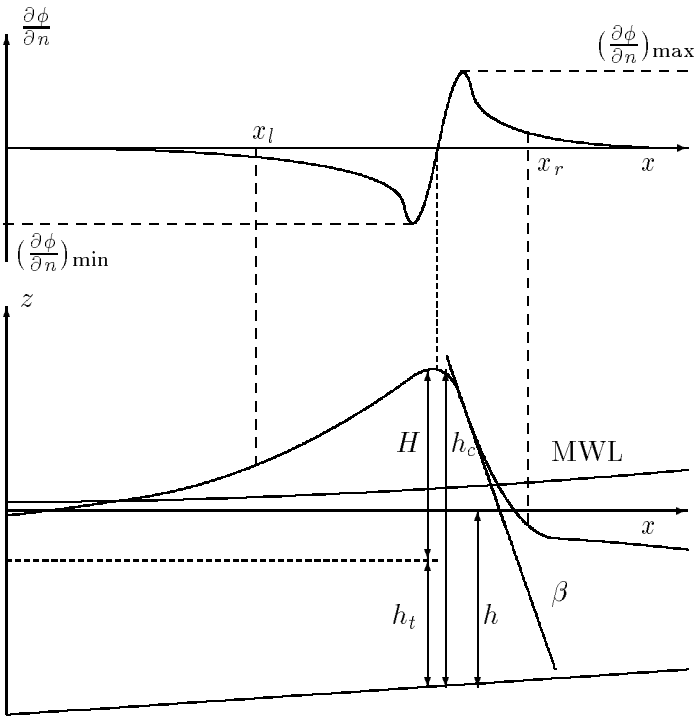

Fig. 2 : Definition of geometric parameters for the breaker model. Note, H is defined as the height between a crest and the previous trough, as in Hansen and Svendsen (1979).

Wave energy absorption

Following Clément (1996) and others, GH implemented an absorbing beach (AB) in the NWT in which an external absorbing pressure $p_f=p_a$ is specified in the dynamic free surface condition (3) (with $z=\eta$), to create a negative work, and thus absorb wave energy over a given section of the free surface (for $x>x_a$). To create additional wave reduction through de-shoaling, the bottom geometry within the AB is specified somewhat similar to a natural bar, with a depth increasing to $h=h_1$ (Fig. 1).

The AB absorbing pressure is specified proportional to the normal particle velocity on the free surface,

$$p_a(x,\eta,t) = \nu_a(x)\,\frac{\partial\phi}{\partial n}(\eta(x,t)) \tag{6}$$

in which ν_a, the beach absorption function, is smoothly varied along the AB as, e.g.,

$$\nu_a(x) = \nu_{ao}\,\rho\sqrt{g h_1}\,(\frac{x-x_a}{l})^2 \tag{7}$$

where ν_{ao} is a non-dimensional beach absorption coefficient, and l is the AB length.

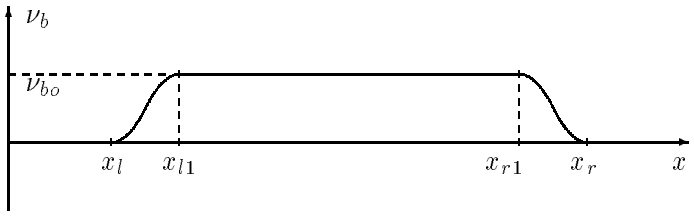

Fig. 3 : Breaker model absorbing pressure shape function.

The same method is now used to selectively absorb energy from breaking waves, for $x \le x_a$ (Fig. 1), while the AB is still used to absorb residual wave energy exiting at the top of the slope, for $x > x_a$. A wave tracking algorithm (detailed below) first identifies breaking waves, within the incident wave train, based on a breaking criterion. The breaker model is assumed to extend from the crest of each breaking wave to two points on each side of the crest where $|\frac{\partial\phi}{\partial n}/(\frac{\partial\phi}{\partial n})_{\min,\max}| > \varepsilon$ $(x_l \le x \le x_r)$, where ε is a small threshold value (Fig. 2). [$|(\frac{\partial\phi}{\partial n})_{\min,\max}|$ are defined as the maximum absolute normal velocity for each side of the wave.] Over each breaker, the absorbing pressure is defined as, $p_f = p_{bm}$, with,

$$p_{bm}(x,\eta,t) = \nu_{bm}(x)\,\frac{\partial\phi}{\partial n}(\eta(x,t)) \tag{8}$$

in which $\nu_{bm} = \nu_{bo}\,S(x)$, with $S(x)$ a breaker shape function providing a smooth transition from areas without the absorbing pressure, to the breaker regions over each breaking wave (Fig. 3). [This function is simply assumed to vary sinusoidally between 0 and 1 over a fraction α of the total breaker length $(x_r - x_l)$; thus, $x_{l1} = x_l + \alpha(x_r - x_l)$ and $x_{r1} = x_r - \alpha(x_r - x_l)$ in Fig. 3.]

The instantaneous power dissipated by each breaking wave is given by,

$$\mathcal{P}_b = \int_{x_l}^{x_r} p_b \frac{\partial\phi}{\partial n}\mathrm{d}\Gamma = \nu_{bo}\int_{x_l}^{x_r} S(x)\left(\frac{\partial\phi}{\partial n}\right)^2 \mathrm{d}\Gamma \tag{9}$$

and is assumed to be proportional to the power dissipated in a turbulent hydraulic jump (e.g., Lamb, 1932, p 280). We find after some transformations,

$$\mathcal{P}_h = \rho\,g\,c\,\frac{h\,H^3}{4\,h_c\,h_t} \tag{10}$$

where H denotes the wave height, h_t the water depth below trough, $h_c = h_t + H$ the water depth below crest (Fig. 2), and (here) c is the absolute wave crest phase speed. We define, $\mathcal{P}_{bm} = \mu\,\mathcal{P}_h$, with $\mu \simeq 1.5$ (e.g., Svendsen *et al.*, 1978) a coefficient to be calibrated based on laboratory experiments. All calculations done, the instantaneous value of each breaker absorption coefficient ν_{bo} is found as a function of both wave and breaker parameters $(H, c, h_t, h, \mu, \varepsilon, \alpha)$, and the wave shape in between x_l and x_r (Figs. 2 and 3).

Wave tracking algorithm and breaking criteria

A free surface tracking algorithm is applied for each time t to determine characteristics of both non-breaking and breaking waves. First, (x, z) locations of local maxima and minima in surface elevation $\eta(x,t)$ are identified (using the high-order geometric representation of the free surface modeled in the BEM). The crest of each wave is calculated as the highest elevation in between two successive minima in surface elevation (i.e., wave troughs). A wave is identified only if its height H is greater than a specified fraction of the incident wave height H_o (typically one-tenth). This avoids including secondary wave crests created during shoaling by nonlinear effects.

Now, for each wave identified this way at time t, the algorithm finds which wave $i = 1, \ldots$ it corresponded to at the previous iteration, at time $t - \Delta t$. The search for the right wave is accelerated by extrapolating the crest position of each earlier wave i, to time t, as,

$$\tilde{x}_c^i(t) \simeq x_c^i(t - \Delta t) + c^i\,\Delta t \tag{11}$$

where, $c^i \simeq \frac{\partial\phi}{\partial t}(x_c^i)/\frac{\partial\phi}{\partial n}(x_c^i)$ is the i's wave crest celerity at time $t - \Delta t$ (assuming a permanent form for the wave over time Δt), and comparing it to the crest position $x_c(t)$ found for the current wave under consideration. Wave heights $H^i(x,t)$ is saved for each wave after final identification has been made, as well as other geometric parameters needed to calculate the hydraulic jump power dissipation using Eq. (10). Crest trajectories $x_c^i(t)$ are calculated for each incident wave, and celerities $c^i(x_c^i, t)$ are calculated as the time derivatives of these. Wavelengths are readily found as $L^i = c^i\,T$, assuming a constant wave period.

A breaking criteria is checked for each wave i identified at time t. Here, a simple wave front slope criteria (Schäffer *et al.*, 1993) is checked, such as $\beta > \beta_{\max}$, to decide whether a wave breaks or not. For those waves j that break, the procedure described in the previous section is applied to calculate the interval $x_l^j \le x \le x_r^j$, in between which the absorbing pressure p_{bm}^j is applied (Fig. 2), according to Eq. (8).

Note that, due to the cold start of computations in the NWT, a larger wave is usually created at the front of the initial wave train. To properly dissipate the energy of this wave before it reaches the top of the slope, the absorbing pressure is applied on it from the toe of the slope onward.

Numerical model

In the NWT, Eq. (1) is transformed into a Boundary Integral Equation (BIE), using Green's 2nd identity, and solved by a

Boundary Element Method (BEM). The BIE is expressed for N discretization nodes on the boundary, and M higher-order elements are defined to interpolate in between discretization nodes. In the present applications, quadratic isoparametric elements are used on lateral and bottom boundaries, and cubic elements ensuring continuity of the boundary slope are used on the free surface. In these elements, referred to as Middle Interval Interpolation (MII) elements, both geometry and field variables are interpolated between each pair of nodes, using the middle-section of a four-node "sliding" isoparametric element. Expressions of BEM integrals (regular, singular, quasi-singular) are given in GSS, GS, and Grilli and Subramanya (1994,1996), for both isoparametric and MII elements.

Free surface boundary conditions (2) and (3) are time integrated based on two second-order Taylor series expansions expressed in terms of a time step Δt and of the Lagrangian time derivative, D/Dt, for ϕ and $\mathbf{R}$. First-order coefficients in the series correspond to free surface conditions (2) and (3), in which ϕ and $\partial\phi/\partial n$ are obtained from the BEM solution of the BIE for (ϕ, $\partial\phi/\partial n$) at time t. Second-order coefficients are expressed as D/Dt of Eqs. (2) and (3), and are calculated using the solution of a second BIE for ($\partial\phi/\partial t$, $\partial^2\phi/\partial t\partial n$), for which boundary conditions are obtained from the solution of the first BIE and the time derivative of Eqs. (3) to (5). Detailed expressions for the Taylor series are given in GSS.

At each time step, global accuracy of computations is verified by computing errors in total volume and energy for the generated wave train. GS showed that these errors are function of both the size (i.e., distance between nodes) and the degree (i.e., quadratic, cubic,...) of boundary elements used in the spatial discretization, and of the size of the selected time step. They proposed a method for adaptively selecting the optimal time step, based on a mesh Courant number $\mathcal{C}_o(t)$. For the MII elements, Grilli and Subramanya (1996) showed that the optimum value of $\mathcal{C}_o$ is around 0.45. This value is used in the present applications.

In computations involving finite amplitude waves, mean drift currents occur ("Stokes drift") which continuously move discretization nodes/Lagrangian markers forward in the NWT. Grilli and Subramanya (1996) developed regridding methods in which nodes can be redistributed at constant arclength intervals over specified regions of the free surface. This method was used to both refine the discretization within the jets of breaking solitary waves and rediscretize areas close to wavemakers, which otherwise would gradually loose their resolution due to forward node motion (GH). Stokes drift and the need for regridding are also experienced in the present computations. However, to limit the number of nodes on the free surface and the computational cost, the initial horizontal node spacing Δx_o on the free surface is gradually reduced over the slope, to match the reduction in wavelength due to shoaling and maintain a node density of at least 15 nodes per waves (from an initial 20 nodes per wavelength over the constant depth part of the NWT). Hence, Grilli and Subramanya's method of constant arclength regridding can not be applied. Instead, a new regridding method was developed in which the initial ratio of each BEM element length to the total length of the free surface is maintained for all times. This method is applied every ten time steps in the present computations. It was verified that regridding only very slightly increased numerical errors on mass conservations at a given time step. However, without regridding, computations would rapidly fail as discretization nodes would keep accumulating downstream in the NWT.

APPLICATIONS

The breaker model is validated by comparing numerical results to laboratory experiments by Hansen and Svendsen (1979), for periodic waves with : $H_o = 0.095$ m (at the toe of the slope), $T = 1$ s, and $h_o = 0.36$ m, shoaling over a $s = 1/34.26$ plane slope for $x \geq 14.78$ m (Fig. 1). [Note, this is also one of the cases used by Skotner and Apelt (1999ab).] In the experiments, waves were generated by a piston wavemaker at $x = 0$, using a second-order wave generation method. Variations of wave-averaged, wave height H, mean-water-level (MWL) $\overline{\eta}$, and celerity c, were measured as a function of x. The same tank geometry and wave characteristics are used in the NWT. Due to the lack of details provided on the second-order wave generation method, wave generation was achieved in the NWT using a piston wavemaker (as in the experiments), moved according to a first-order cnoidal wave solution, with wave height 0.095 m. It was observed that generated waves slightly adjusted their shape and height as they propagated over constant depth down the NWT, likely due to nonlinear effects (as discussed by Svendsen and Grilli (1990) and GH). The incident wave finally reached a stabilized height $H_o = 0.083$ m at the toe of the slope in the NWT, i.e., a smaller value than in the corresponding experiments (which used a wave height 0.1 m at the wavemaker). Rather than repeating these quite demanding computations with a larger incident wave, the comparison of numerical results with experiments is carried out using these slightly smaller generated waves. It is planned to repeat these computations at a later time, using a streamfunction wave generation, for which no change in wave height should occur over constant depth (GH).

An absorbing beach, with water depth deepening to $h_1 = 0.3$ m, is specified at the top of the slope (Fig. 1). The AB is located for $x \geq x_a = 25.96$ m and $x \leq 30$, with $\nu_{ao} = 0.01$. The minimum depth on the slope at $x = x_a$ is $h_a = 0.0343$ m. In the breaker model, breaking is assumed to occur when the maximum wave front slope reaches $\beta_{\max} = 37^o$, with $\alpha = 0.1$, and $\varepsilon = 10^{-5}$. Finally, as recommended by Svendsen *et al.* (1978), we select $\mu = 1.5$.

BEM discretization parameters are $N_f = 315$ nodes on the free surface, with 314 MII sliding cubic elements of initial length Δx_o varying from 0.1 m at the wavemaker down to 0.025 m at $x = 30$. Quadratic 3-node isoparametric elements are used on the other parts of the boundary. There is a total of $N = 672$ nodes on the boundary and $M = 491$ elements. The initial time step is $\Delta t_o = 0.01$ s, which is

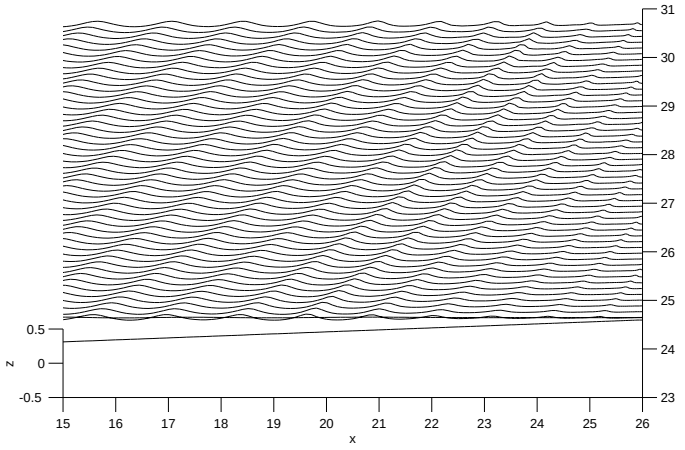

Fig. 4 : Stack diagram of computed surface elevations as a function of time (rightward axis) for a cnoidal wave with : $H_o = 0.083$ m, $T = 1$ s, and $h_o = 0.36$ m, over a $s = 1{:}34.26$ slope.

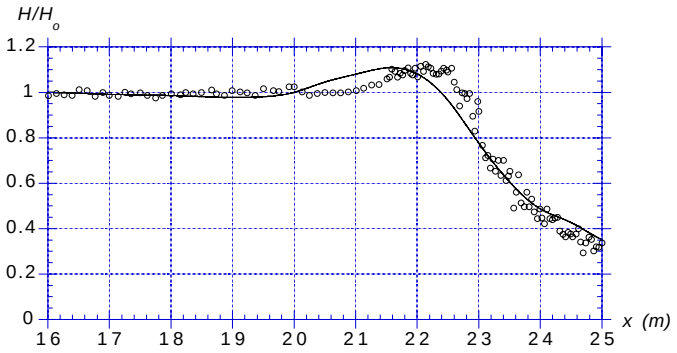

Fig. 5 : Same case as Fig. 4. Calculated mean wave height (——). (∘) are experimental data from Hansen and Svendsen (1979), for $H_o = 0.095$ m.

consistent with a Courant number equal to 0.45 for $x < 26$ m (Grilli and Subramanya, 1996). A total of 5000 time steps were run in these computations. The relative error on the NWT initial volume ($V_o = 8.322\,\mathrm{m}^3/\mathrm{m}$) was only 0.011% after 3500 iterations, at time $t = 21$ s. At this stage, the NWT reached an almost steady state in which larger waves kept entering the AB from the top of the slope. This led to somewhat larger numerical errors. After 5000 iterations, at time $t = 30.04$ s the volume error increased to 0.087%, which is still quite small (Fig. 8).

Figs. 4-7 show results of computations. Fig. 4 shows stacked free surface elevations calculated as a function of time, for $t > 24.5$ s, i.e., after computations in the NWT have reached an almost steady state. Breaking occurs in average for $x_b \simeq 21.5$ m. We clearly see the shoaling region for $x < x_b$, where wavelength decreases and wave height $H(x)$ eventually increases, and the surf-zone region beyond breaking, where H decreases. Crest trajectories $x_c(t)$ are visible as darker curves in the figure. The slope of these

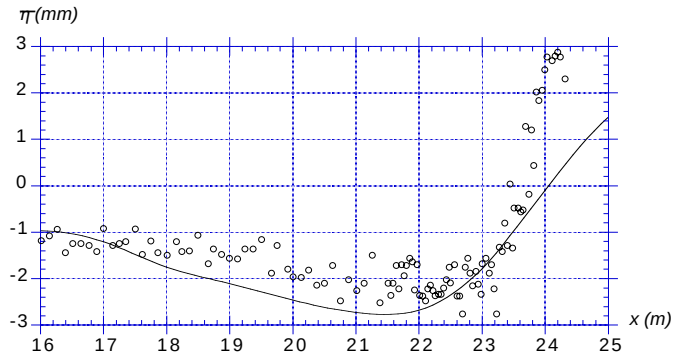

Fig. 6 : Calculated MWL (——), for same case as in Fig. 4-5.

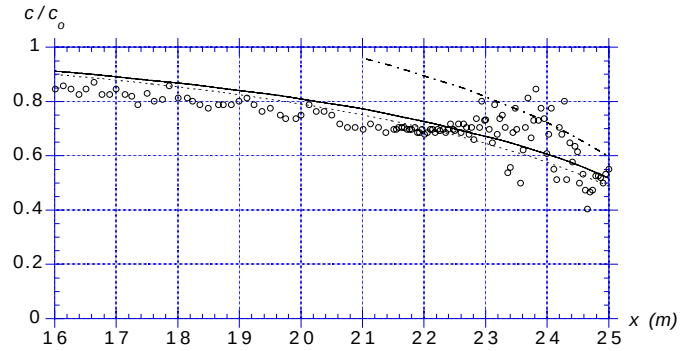

Fig. 7 : Calculated mean wave celerity (———), compared to NSW (— - —) and LWT (- - - - -) celerities, for same case as in Fig. 4-6.

curves provides the wave phase speed as, $c = \mathrm{d}x_c/\mathrm{d}t$.

Fig. 5 shows the calculated average wave height (ensemble average of computations for 6 successive waves), as compared to laboratory experiments. The agreement is quite good, although breaking occurs slightly too early (i.e. for too small an x) in the NWT. Fig. 6 shows the computed average MWL, as compared to experiments. The agreement is also good for $x < 24$ m. Finally, Fig. 7 shows the calculated average celerity, as compared to the celerity predicted by linear wave theory $c_{\mathrm{LWT}} = c_o \tanh kh$ (with $c_o = gT/2\pi = 1.56$ m/s, wavenumber $k = 2\pi/L$, and wavelength $L = cT$), and that of the Nonlinear Shallow Water equations, $c_{\mathrm{NSW}} = \sqrt{g(H+h)}$ (using the FNPF results for H). The agreement of c and c_{LWT} with experiments during the shoaling part ($x < 21.5$ m) is good, considering the difficulties reported by Hansen and Svendsen in accurately measuring celerities, and differences in H_o value. Beyond breaking, experimental results show a larger variance, due to difficulties in identifying foamy crests in the experiments, and the agreement with computations is less good, although still reasonable. NSW equations seem to consistently overpredict wave celerity.

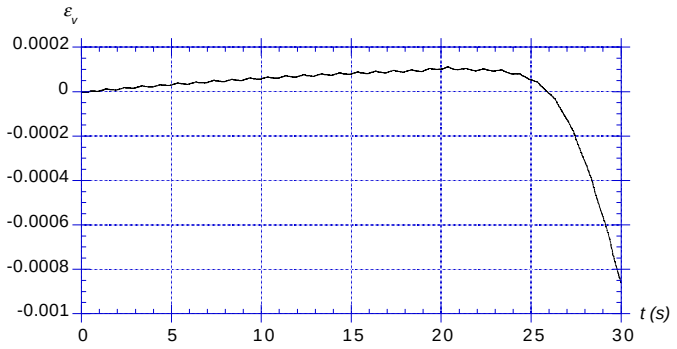

Fig. 8 : Relative error on volume conservation as a function of time in the computations, for same case as in Fig. 4-7.

CONCLUSIONS

Preliminary numerical results reported in this paper indicate that the spilling breaker model implemented in the fully nonlinear NWT correctly accounts for the overall behavior of periodic waves shoaling and breaking over a sloping bottom, i.e., the approximate location and height of breaking, and the rate of energy dissipation in the breakers, leading to a reduction in wave height and to an increase in MWL in the surf-zone. The general agreement of numerical and experimental results confirms the relevance of the hydraulic jump analogy, using $\mu = 1.5$, to model the instantaneous power dissipated in spilling breakers, although it is hard to assess whether this μ value is general unless more cases are tested. In particular, in the one case reported here (Figs. 5-7), an increased dissipation in post-breaking waves (i.e., a larger μ) would reduce H and increase $\overline{\eta}$,thus providing a better agreement with experiments.

The $\beta_{\max}$ value used in the breaking criteria was larger than that used in Boussinesq models (e.g., Schäffer *et al.*, 1993). This is because the fully nonlinear NWT can model steeper waves than Boussinesq models and thus delay the onset of breaking. Nevertheless, for the reported case, breaking still occurs too soon and it would be of interest to try and increase $\beta_{\max}$ further. A limitation however is that, with too large a $\beta_{\max}$ value, it may be hard to quickly enough absorb wave energy and prevent wave overturning from occurring. Clearly more work needs to be done on the sensitivity of results to this important parameter.

Experimental and FNPF results show effects of amplitude dispersion, which leads to a larger celerity, the larger the wave (Fig. 7). Note that FNPF computations with this model, for solitary wave overturning on mild slopes, reported by Wei *et al.* (1995), predicted celerity variations similar to experimental results in Fig. 7, i.e., sharply increasing just after breaking. In those computations, however, the breaker jet was finely resolved and the rise in (crest) celerity resulted from the rapid forward motion of the jet (which actually is prevented from forming in the present case).

Future work will also concentrate on running more of the 17 different incident waves tested by Hansen and Svendsen (1979) in the NWT and further calibrating the breaker model parameters based on these results. We will also compare velocities predicted under breaking waves to laboratory measurements (e.g., Veeramony and Svendsen, 2000). Finally, as mentioned above, it appears that the streamfunction wave generation may offer a more accurate means of simulating experimental conditions in the NWT.

In conclusion, the NWT, with the addition of a simple breaker model, has the potential for realistically simulating wave shoaling from deep water to shore, up to breaking over a sloping bottom geometry, with the possibility of studying effects of bottom obstacles and irregularities. One should, however, keep in mind the limitations of the method for modeling details of the flow in breaking waves.

ACKNOWLEDGMENT

This research was supported by the Office of Naval Research, under grant N00014-99-1-0439 from the US Department of the Navy, Office of the Chief of Naval Research. Anonymous reviewers are thanked for making interesting suggestions.

REFERENCES

Clément, A. (1996). "Coupling of two absorbing boundary conditions for 2D time-domain simulations of free surface gravity waves," *J. Comp. Phys.*, Vol 26, pp 139-151.

Cointe, R. and M.P., Tulin (1994). "A theory of steady breakers," *J. Fluid Mech.*, Vol 276, pp 1-20.

Dold, J.W. and D.H., Peregrine (1986) "An efficient boundary integral method for steep unsteady water waves," In *Numerical methods for Fluid Dynamics II* (ed. K.W. Morton & M.J. Baines), pp 671-679, Clarendon Press, Oxford.

Gentaz, L.and B. Alessandrini (2000) "Detection of wave breaking in a 2D viscous numerical wave tank, " in *Proc. 10th Offshore and Polar Engng. Conf.*, Vol III, 263-270.

Grilli, S.T., Guyenne, P. and F., Dias (2001). "A fully nonlinear model for three-dimensional overturning waves over arbitrary bottom," *Intl. J. Numer. Methods in Fluids*, Vol 34, 39 pps (in press).

Grilli, S.T. and J. Horrillo (1997a). "Numerical generation and absorption of fully nonlinear periodic waves," *J. Engng. Mech.*, Vol 123(10), pp 1060-1069.

Grilli, S.T. and J., Horrillo (1997b). "Fully nonlinear properties of periodic waves shoaling over mild slope," *Proc. 25th Intl. Conf. on Coastal Engng.*, Vol 1, pp 717-730. ASCE edition.

Grilli, S.T. and J., Horrillo (1999) "Shoaling of periodic waves over barred-beaches in a fully nonlinear numerical wave tank," *Intl. J. Offshore and Polar Engng.*, Vol 9(4), pp 257-263.

Grilli, S.T., Skourup, J. and I.A., Svendsen (1989) "An efficient boundary element method for nonlinear water waves," *Engng. Analysis with Boundary Elements*, Vol 6(2), pp 97-107.

Grilli, S.T. and I.A., Svendsen (1990) "Corner problems and global accuracy in the boundary element solution of nonlinear wave flows," *Engng. Analysis with Boundary Elements,* Vol 7(4), pp 178-195.

Grilli, S.T., Svendsen, I.A. and R., Subramanya (1997) "Breaking criterion and characteristics for solitary waves on slopes," *J. Waterway Port Coastal and Ocean Engng.,* Vol 123(3), pp 102-112.

Grilli, S.T., Svendsen, I.A. and R., Subramanya (1998) "Closure of : breaking criterion and characteristics for solitary waves on slopes," *J. Waterway Port Coastal and Ocean Engng.,* Vol 124(6), pp 333-335.

Grilli, S.T. and R., Subramanya (1994) "Quasi-singular integrations in the modeling of nonlinear water waves," *Engng. Analysis with Boundary Elements,* Vol 13(2), pp 181-191.

Grilli, S.T. and R., Subramanya (1996) "Numerical modeling of wave breaking induced by fixed or moving boundaries," *Comput. Mech.,* Vol 17, pp 374-391.

Grilli, S.T., Subramanya, R., Svendsen, I.A. and J., Veeramony (1994) "Shoaling of solitary waves on plane beaches," *J. Waterway Port Coastal and Ocean Engng.,* Vol 120(6), pp 609-628.

Guignard, S., Grilli, S.T., Marcer, R. and V., Rey (1999) "Computation of shoaling and breaking waves in nearshore areas by the coupling of BEM and VOF methods," In *Proc. 9th Offshore and Polar Engng. Conf.*, Vol III, 304-309.

Guignard, S., Marcer, R., Rey, V., Kharif, Ch., and Ph. Fraunié (2001) "Solitary wave breaking on sloping beaches : 2D two-phase flow numerical simulation by SL-VOF method," *Eur. J. Mech.* (in press).

Hansen, J.B. and I.A., Svendsen (1979) "Regular waves in shoaling water. Experimental data," *Series paper no. 21.* Institute of Hydrodynamics and Hydraulic Engng. Tech. Univ. of Denmark.

Karambas, T.V. and C., Koutitas (1992) "A breaking wave propagation model based on the Boussinesq equations," *Coastal Engng.,* Vol 18, pp 1-19.

Kennedy, A.B., Chen, Q., Kirby, J.T., and R.A., Dalrymple (2000) "Boussinesq modeling of wave transformation, breaking, and runup. I: 1D," *J. Waterway Port Coastal and Ocean Engng.,* Vol 126(1), pp 39-47.

Lamb, H. (1932) *Hydrodynamics.* Cambridge Univ. Press.

Lin, P. and P.L.F. Liu (1998) "A numerical study of breaking waves in the surf zone," *J. Fluid Mech.,* Vol 359, pp 239-264.

Longuett-Higgins, M.S. and E.D., Cokelet (1976) "The deformation of steep surface waves on water - I. A numerical method of computation," *Proc. R. Soc. Lond.,* Vol A350, pp 1-26.

Madsen, P.A., Sorensen, O.R., and H.A., Schäffer (1997) "Surf zone dynamics simulated by a Boussinesq type model. Part I. Model description and cross-shore motion of regular waves," *Coastal Engng.,* Vol 32, pp 255-287.

Nadaoka, K. and O., Ono (1999) "Time-dependent depth-integrated turbulence modeling of breaking waves," In *Proc. 26th Intl. Conf. on Coastal Engng.*, Vol 1, pp 86-97.

Ohyama, T. and K., Nadaoka (1991) "Development of a numerical wave tank for analysis of nonlinear and irregular wave fields," *Fluid Dyn. Res.,* Vol 8, pp 231-251.

Raad, P.E. (1997) "Modeling tsunamis with marker and cell methods," Chapter in *Long-Wave Runup Models*, pps. 181-203. World Sc. Publ.

Schäffer, H.A., Madsen, P.A., and R., Deigaard (1993) "A Boussinesq model for wave breaking in shallow water," *Coastal Engng.,* Vol 20, pp 185-202.

Skotner, C. and C.J. Apelt (1999a) "Application of a Boussinesq model for the computation of breaking waves. Part 1 : Development and verification," *Ocean Engng.,* Vol 26, pp 907-926.

Skotner, C. and C.J. Apelt (1999b) "Application of a Boussinesq model for the computation of breaking waves. Part 2 : Wave-induced setdown and setup on a submerged coral reef," *Ocean Engng.,* Vol 26, pp 927-947.

Subramani, A.K., Beck, R.F. and W.W. Schultz (1998) "Suppression of wave breaking in nonlinear water wave computations," in *Proc. 13th Intl. Work. Water Waves and Float. Bodies*, pp 139-141. Delft Univ.

Svendsen, I.A. and S.T., Grilli (1990) "Nonlinear waves on steep slopes," *J. Coastal Res.,* SI 7, pp 185-202.

Svendsen, I.A. and P.A., Madsen (1984) "A turbulent bore on a beach," *J. Fluid Mech.,* Vol 148, pp 73-96.

Svendsen, I.A., P.A., Madsen and J.B. Hansen (1978) "Wave characteristics in the surf zone," in *Proc. 16th Intl. Coastal Engng. Conf.*, pp 521-539.

Svendsen, I.A., Veeramony, J., Bakunin, J. and J.T. Kirby (2001) "The flow in weal turbulent hydraulic jumps," *J. Fluid Mech.* (submitted).

Veraamony, J. and I.A., Svendsen (1999) "A Boussinesq model for breaking waves : comparisons with experiments," In *Proc. 26th Intl. Conf. on Coastal Engng.*, Vol 1, pp 258-271.

Veraamony, J. and I.A., Svendsen (2000) "The flow in surf-zone waves," *Coastal Engng.*, Vol 39, pp 93-122.

Tanaka, M. (1986). "The stability of solitary waves," *Phys. Fluids,* Vol 29(3), pp 650-655.

Vinje, T. and P., Brevig (1981) "Numerical simulation of breaking waves," *Adv. Water Res.,* Vol 4, pp 77-82.

Wang, P., Yao, Y. and M.P., Tulin (1995) "An efficient numerical tank for non-linear water waves, based on the multi-subdomain approach with BEM," *Intl. J. Num. Methods in Fluids,* Vol 20, pp 1315-1336.

Wei, J., Kirby , J.T, Grilli, S.T. and R., Subramanya (1995) A fully nonlinear Boussinesq model for surface waves. Part 1. Highly nonlinear unsteady waves. *J. Fluid Mech.*, Vol 294, pp 71-92.